Supplementary Information of "Probing the interlayer excitation dynamics in WS_2/WSe_2 heterostructures with broadly tunable pump and probe energies"

Anran Wang,[a] Wendian Yao,[b] Zidi Yang,[b] Dingqi Zheng,[a] Songlin Li,[a] Yi Shi,[a] Dehui Li[b] and Fengqiu Wang*[a]

[a]School of Electronic Science and Engineering, Nanjing University, Nanjing 210093, China, Emails: fwang@nju.edu.cn

[b]School of Optical and Electronic Information, Huazhong University of Science and Technology, Wuhan 430074, China

Supplementary Note 1. Second harmonic generation (SHG) measurements of the WS_2/WSe_2 heterostructure

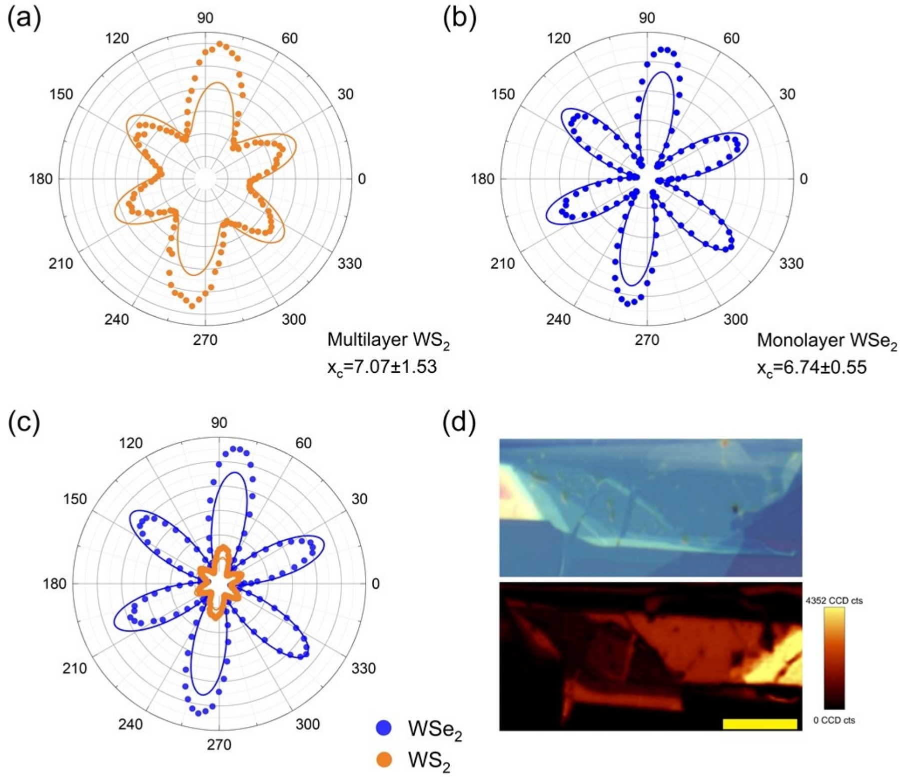

Figure S1 Polarization-dependent SHG of (a) multilayer WS_2 and (b) monolayer WSe_2. (c) The sum of individual layers of WS_2/WSe_2 heterostructure. The experimental and fitting results are plotted as solid circles and lines, respectively. (d) SHG mapping of the WS_2/WSe_2 heterostructure. The scale bar is 10 μm.

The SHG measurements of the WS_2/WSe_2 heterostructure is shown in Fig. S1. Though bare individual monolayer WS_2 is absent in the sample, the crystalline orientation of adjacent multilayer was determined. According to the sine function fitting results, the WSe_2 and WS_2 in our sample can be identified to be closely aligned. To further identify the twist angle of the WS_2/WSe_2 heterostructure, SHG mapping is performed and is shown in Fig. S1d. As compatible with previous results, the SHG intensity of the heterojunction region is significantly weaker than that of the monolayer region, suggesting the WSe_2 and WS_2 are nearly 60° aligned. The SHG image was acquired using WITec alpha300 R imaging microscope, equipped with a 1064 nm picosecond laser from NPI Lasers.

Supplementary Note 2. Pump-probe measurement of monolayer WSe_2 in the sample, using femtosecond transient reflectance setup

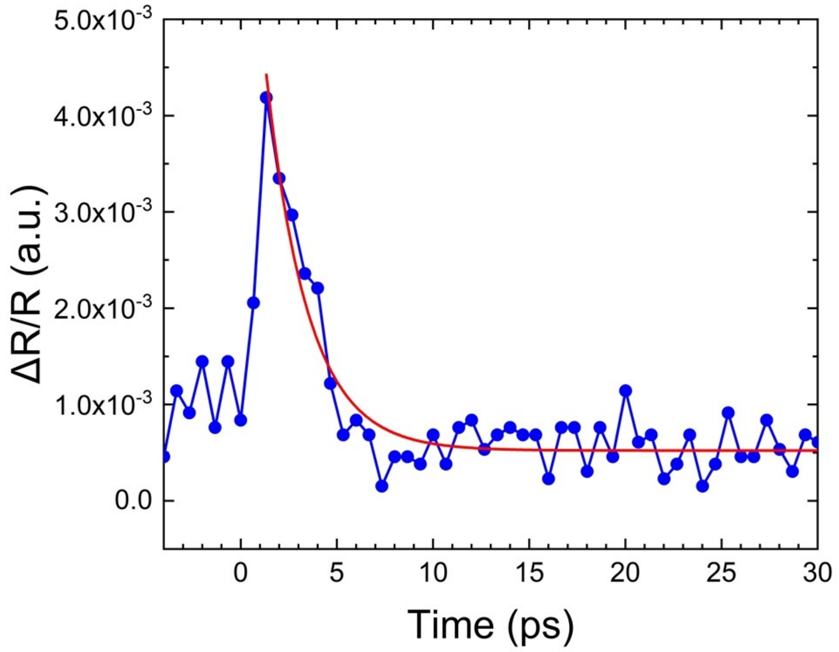

Figure S2 The transient reflectance of monolayer WSe_2 deposited on h-BN flakes at 7 K, with the pump wavelength of 655 nm and probe wavelength of 785 nm. The measurements were performed at back-gate voltage of 0 V.

Fig. S2 shows the relaxation dynamics of monolayer WSe_2 with a h-BN passivation flake under low temperature. An ultrafast lifetime of ~ 2.2±0.2 ps in the monolayer WSe_2 can be observed.

Supplementary Note 3. Back-gated voltage-dependent pump-probe measurements of the WS_2/WSe_2 heterostructure

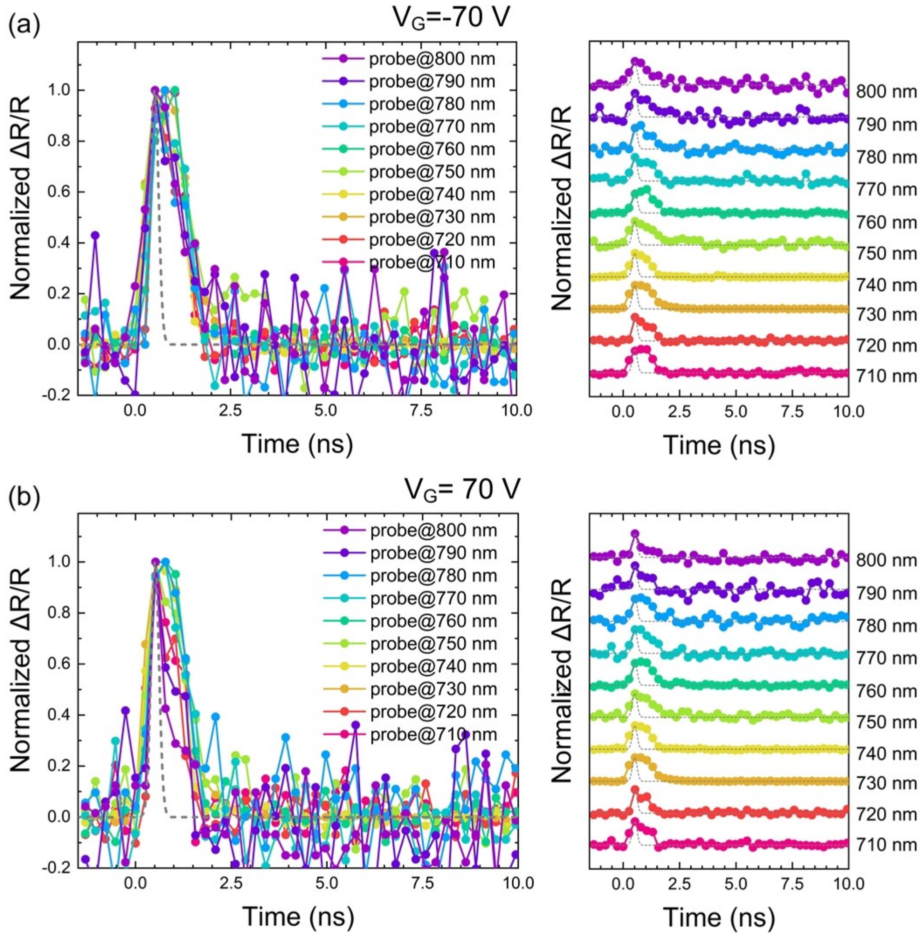

Figure S3 (a) Normalized transient reflectance of WS_2/WSe_2 heterostructure under the back-gate voltage of -70 V. (b) Normalized transient reflectance of WS_2/WSe_2 heterostructure under the back-gate voltage of 70 V. The gray dashed line represents the IRF of ~247 ps for the picosecond excitation setup. All measurements are performed at 7 K.

To reveal the influence of the background carrier concentration on the transient dynamics, the relaxation dynamics of interlayer excitation in the WS_2/WSe_2 heterostructure has been measured with varying back-gate voltages. As shown in Fig. S3, the observed transient features of interlayer excitation remain consistent under different back-gate voltage. The time constants are similar to the ones with a zero back-gate voltage.

Supplementary Note 4. Pump-probe measurement of the WS_2/WSe_2 heterostructure with probe energy resonant with the interlayer exciton transitions

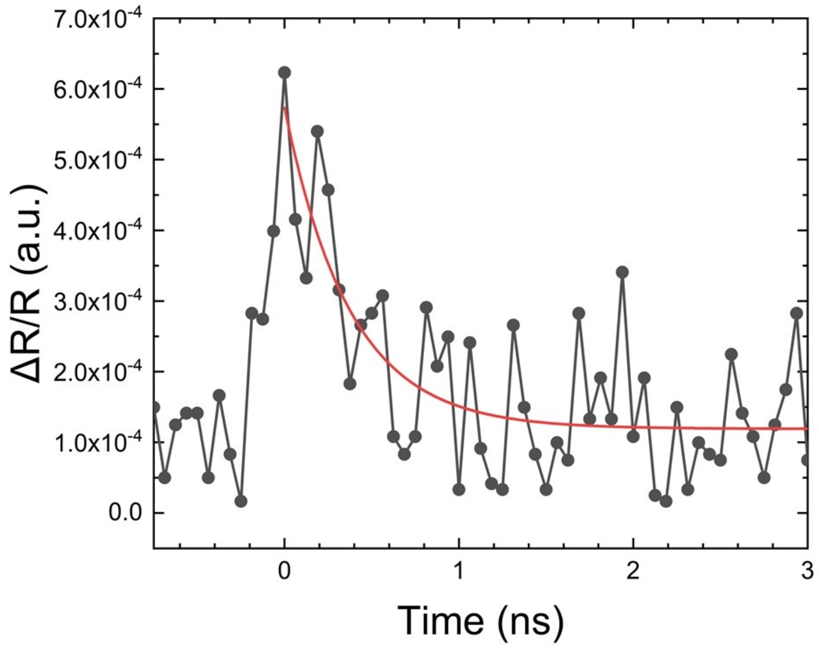

Figure S4 Transient reflectance of WS_2/WSe_2 heterostructure at 7 K, with the pump wavelength of 655 nm and probe wavelength of 852 nm. The measurements were performed at a back-gate voltage of 0 V.

Fig. S4 shows the interlayer exciton dynamics of WS_2/WSe_2 heterostructure with a probe energy resonant with the interlayer exciton transition. The lifetime of the interlayer excitons as inferred by the transient reflectance is about 376±72 ps. Due to the small oscillator strength of interlayer exciton, the signal-to-noise ratio of the transient reflectance data is relatively poor.